Available online at www.sciencedirect.com
SCIENCE DIRECT®
Ecological Modelling 183 (2005) 157–172
ECOLOGICAL MODELLING
www.elsevier.com/locate/ecolmodel

Influence of topographic complexity on solar insolation estimates for the Colorado River, Grand Canyon, AZ

Michael D. Yard[a,*], Glenn E. Bennett[a], Steve N. Mietz[a], Lewis G. Coggins Jr.[a], Lawrence E. Stevens[b], Susan Hueftle[a], Dean W. Blinn[c]

[a] *Grand Canyon Monitoring and Research Center, U.S. Geological Survey, Flagstaff, AZ 86001-1600, USA*
[b] *Grand Canyon Wildlands Council, Flagstaff, AZ 86001-5467, USA*
[c] *Department of Biological Sciences, Northern Arizona University, Flagstaff, AZ 86011-5640, USA*

Received 22 July 2003; received in revised form 4 May 2004; accepted 12 July 2004

Abstract

Rugged topography along the Colorado River in Glen and Grand Canyons, exemplifies features common to canyon-bound streams and rivers of the arid southwest. Physical relief influences regulated river systems, especially those that are altered, and have become partially reliant on aquatic primary production. We measured and modeled instantaneous solar flux in a topographically complex environment to determine where differences in daily, seasonal and annual solar insolation occurred in this river system. At a system-wide scale, topographic complexity generates a spatial and temporal mosaic of varying solar insolation. This solar variation is a predictable consequence of channel orientation, geomorphology, elevation angles and viewshed. Modeled estimates for clear conditions corresponded closely with observed measurements for both instantaneous photosynthetic photon flux density (PPFD: μmol m^{-2} s^{-1}) and daily insolation levels (relative error 2.3%, CI $\pm$0.45, S.D. 0.3, n = 29,813). Mean annual daily insolation levels system-wide were estimated to be 36 mol m^{-2} d^{-1} (17.5 S.D.), and seasonally varied on average from 13.4–57.4 mol m^{-2} d^{-1}, for winter and summer, respectively. In comparison to identical areas lacking topographic effect (idealized plane), mean daily insolation levels were reduced by 22% during summer, and as much as 53% during winter. Depending on outlying topography, canyon bound regions having east–west (EW) orientations had higher seasonal variation, averaging from 8.1 to 61.4 mol m^{-2} d^{-1}, for winter and summer, respectively. For EW orientations, 70% of mid-channel sites were obscured from direct incidence during part of the year; and of these sites, average diffuse light conditions persisted for 19.3% of the year (70.5 days), and extended upwards to 194 days. This predictive model has provided an initial quantitative step to estimate and determine the importance of autotrophic production for this ecosystem, as well as a broader application for other canyon systems.

Keywords: Solar incidence; PPFD; Topographic relief; GIS; Aquatic

* Corresponding author. Tel.: +1 928 779 1856.
E-mail address: myard@infomagic.net (M.D. Yard).

0304-3800/$ – see front matter © 2004 Published by Elsevier B.V.
doi:10.1016/j.ecolmodel.2004.07.027

1. Introduction

Vertical relief interferes with incoming solar incidence and can dramatically affect ecosystem energetics, particularly in canyon-bound regions or along densely vegetated streams (Vanote et al., 1980; Hawkins et al., 1982; Monteith and Unsworth, 1990). Physical obstructions are recognized for having pronounced effects on daily, seasonal, and annual solar insolation levels (Hill, 1996). Subtle differences in altitude angles, elevation surface gradients, skylight, and orientation generate varying levels of spatio/temporal complexity (Kumar et al., 1997; Dozier and Frew, 1990). In GIS-modeled environments, solar radiation models have been used effectively to estimate insolation differences on large-scale geographic surfaces (mountainous and canyon terrain) (Dozier and Outclat, 1979; Rich et al., 1995). However, studies on topographic effects in river ecosystems are uncommon, owing perhaps to methodological constraints (e.g., grid-size limitations, sampling devices) used to determine photosynthetic photon flux density (PPFD: μmol m^{-2} s^{-1}).

The Colorado River (CR) in Glen and Grand Canyons is representative of topographically complex riverine environments in the arid southwestern United States. Because of dam-regulation, some of the biological resources in the CR ecosystem are highly affected (Blinn and Cole, 1991; Stevens et al., 1997a, 1997b), and considerable evidence suggests that this river is light-limited and partially dependent on autotrophic production (Blinn and Cole, 1991; Shaver et al., 1997; Stevens et al., 1997a, 1997b; Blinn et al., 1998; Benenati et al., 2000; Walters et al., 2000; Shannon et al., 2001). This condition is unusual, because most large rivers are primarily an allochthonous based system (Haden et al., 1999); therefore, understanding physical factors limiting PPFD has considerable ecological significance for this and other regulated rivers.

The CR is one of the most regulated large rivers in the US that flows 475 km through northern Arizona between two large reservoirs, Lake Powell and Lake Mead (Stevens et al., 1997a, 1997b). Because suspended-sediment is now sequestered in Lake Powell reservoir, hypolimnetic flows released from Glen Canyon Dam (GCD) are highly transparent. Dam releases typically fluctuate from 142 to 708 m^3 s^{-1} on a diurnal schedule. This is a very turbulent river that flows through an extensive geographic region where suspended-sediment supplied from tributaries limits subaqueous PPFD (Shaver et al., 1997). Yet, these light-attenuating effects are subsequent to the influence that topographic relief has on regulating the quantity of incoming solar incidence received initially at the water surface.

We examined the role topographic relief has on regulating daily, seasonal and annual solar insolation reaching the CR water surface. Geomorphic control functions at regional and local scales to influence the incised characteristics of this canyon dominated river by regulating channel meanders, orientation and topography (Schmidt, 1990; Gregory et al., 1991; Stevens et al., 1997a; Schmidt et al., 1998). Ecologists have faced similar problems in other aquatic systems; yet, beyond general site-specific descriptions empirical efforts are often quantitatively compromised by limited deployment periods or spatial coverage. A number of predictive solar models are available (Dubayah and Rich, 1995; Kumar et al., 1997), although some are incomplete, costly, complicated, or have considerable data requirements. Thus, our study had multiple objectives: (1) develop a generalized model for estimating instantaneous solar flux for large rivers containing topographically complex environments and (2) determine where differences in daily, seasonal and annual solar insolation occurred along the CR.

2. Methods

Study area includes four major canyon sections: Glen Canyon, Marble Canyon, Central Grand Canyon, and Western Grand Canyon (Fig. 1). These larger canyon sections have varying channel widths, heights, and orientations (Stevens et al., 1997a, 1997b). Contained within these major canyon sections are subunits described as geomorphic reaches, each having different topographic, stratigraphic and erosive characteristics (Howard and Dolan, 1981; Schmidt, 1990; Stevens et al., 1997a) (Table 1). Locations are described in relation to distance in river kilometers (Rkm) downstream from GCD (0.0 Rkm).

2.1. Solar and ground incidence

Solar flux is distributed over a broad range of wavelengths and peaks within the visible band

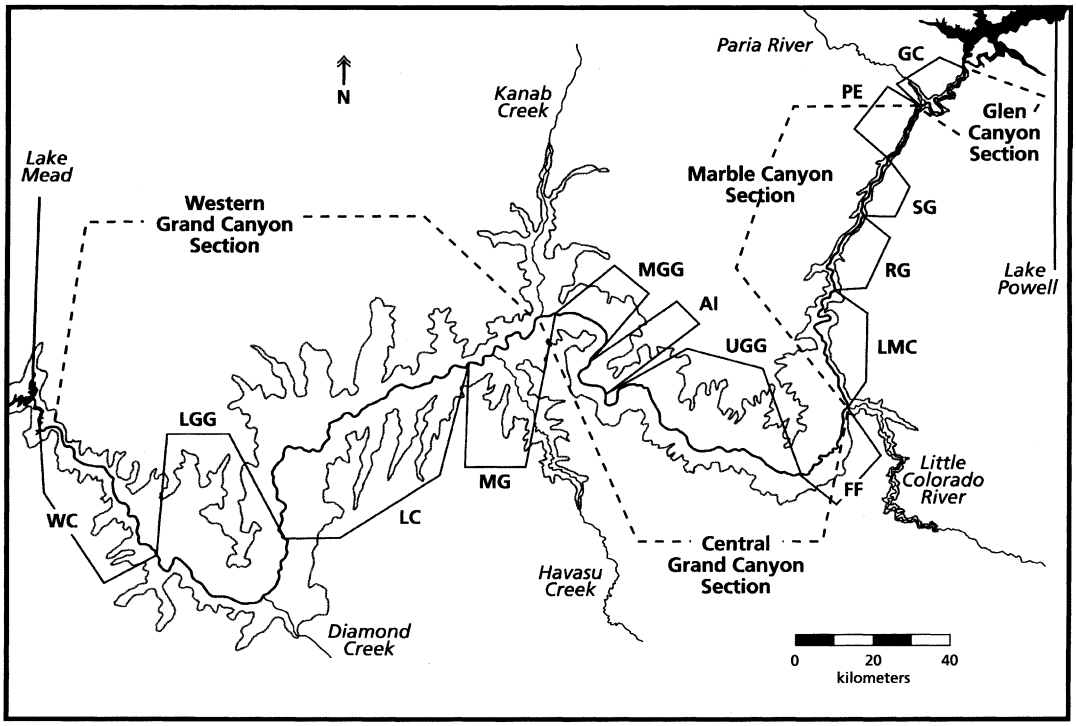

Fig. 1. Map showing major canyon sections, geomorphic reaches, and tributaries of the Colorado River. Estimates of daily solar insolation were calculated at hectometer intervals along the entire river centerline for 474.5 km from Glen Canyon Dam to Lake Mead, AZ.

Table 1
Major canyon sections and geomorphic reaches found along the Colorado River from Glen Canyon Dam to Lake Mead

	River kilometer
Glen Canyon section	0.00–26.8
Marble Canyon section	
Permian (PE)	26.8–43.5
Supai gorge (SG)	43.5–61.7
Redwall gorge (RG)	61.7–83.1
Lower marble Canyon (LMC)	83.1–124.3
Central Grand Canyon section	
Furnace flats (FF)	124.3–149.9
Upper granite gorge (UGG)	149.9–214.9
Aisles (AI)	214.9–227.3
Middle granite gorge (MGG)	227.3–250.5
Western Grand Canyon section	
Muav gorge (MG)	250.5–282.7
Lower Canyon (LC)	282.7–369.4
Lower granite gorge (LGG)	369.4–421.2
Western Canyon (WC)	421.2–474.5

Boundary locations are based on river kilometers (Rkm) in relationship to distance downstream from Glen Canyon Dam.

(400–700 nm), constituting 38.15% of the total solar spectrum (Kirk, 1983). Solar radiation impinging on the earth's outer atmosphere is relatively constant, with exceptions due to differences in solar surface temperature and the earth's elliptical orbit (Jones, 1992). Incidence received at ground level, however, is far from constant and is small relative to total extraterrestrial solar flux. In general, net atmospheric solar flux measured at ground level is less than 5% because of light absorption and scattering from ozone, water vapor, and airborne particles (Cole, 1983; McCullough and Porter, 1971; List, 1971). This ground level incidence is regulated by geometric orientation of the sun relative to the incidental surface. Angular departures from normal (perpendicular to the surface) increases the solar zenith angle, which results in decreasing total solar flux received at the earth's surface (Jones, 1992; Rosenberg et al., 1983). Simple estimates of solar flux (SF) are determined as:

$$SF = SF_N \cos\theta \quad (1)$$

where SF_N is solar flux normal to surface, and θ is zenith angle, representing the angle between the direct beam and normal; therefore as θ increases, SF decreases.

In addition to θ, the depth of the overlying air-mass influences the degree of atmospheric absorption, reflection, and refraction, such that SF decreases exponentially as a function of optical depth (Page and Sharples, 1988; Kasten and Young, 1989). Beer's law describes this relationship as:

$$SF = SF_0 e^{(-Kz)} \tag{2}$$

where SF_0 is initial solar flux, K is coefficient of atmospheric light-attenuation, and SF is resulting intensity after a known optical depth (z) through a given air-mass (Stine and Harrigan, 1985; Kasten and Young, 1989). Yet, accounting for multiple-light attenuating factors requires considerable knowledge of atmospheric conditions (e.g., climate, transmissivity, atmospheric pressure, and cloud cover), and for all practicality atmospheric data are not sufficiently robust or available for most localities (List, 1971). This often precludes using more conventional methods for estimating SF. We used an alternative approach whereby we substituted SF_N for a parameter called normalized ground incidence (GI_N). This parameter represents maximum SF received at ground surface following atmospheric light-attenuation if θ were normal ($\theta = 0^\circ$) and assumes that factors contributing to light-attenuation remain constant. Validity of this assumption is contingent on the variability of local atmospheric conditions. Therefore, constancy of GI_N requires some empirical grounding to determine whether the error varies systematically (spatio/temporal) or within levels acceptable to researchers.

To address this, we used data measured at water surface (LiCor, Inc., LI-190SA) representing PPFD for a wide range of θ angles collected at multiple sites for different years, seasons, and times. We solved for the best estimate of GI_N using a non-linear optimization program and applying a minimization technique that reduced the sum of squared residuals (Frontlines Systems, Inc. 1999).

2.2. Solar coordinates and zenith angle

The above relationships indicate that θ is important for estimating daily solar insolation because the mathematical coordinate system used to estimate solar angles requires knowing the spatio/temporal relationships specific to a site location. Solar coordinates are based on solar time (ST), thus differences among local standard time (LST) and ST must be considered. Converting LST to ST requires two adjustments. The first accounts for differences in longitude among standard meridian L_{ST} and observation location L_{OB}. We used a correction of ± 4 min (i.e., positive east and negative west) for every degree longitude (Rapp, 1981). Secondly, seasonal differences among LST and ST (± 16 min) are related to the earth's elliptical orbit and inclination relative to solar orbital plane. The equation of time (E) accounts for the earth-sun geometric relationship, and is calculated from:

$$E = 9.87 \sin\left[\frac{2(360(\text{Jday} - 81))}{365}\right] - 7.53 \cos\left[\frac{360(\text{Jday} - 81)}{365}\right] - 1.5 \sin\left[\frac{360(\text{Jday} - 81)}{365}\right] \tag{3}$$

where daily differences in ST relative to LST are corrected by Julian date (Jday) (Cousins, 1969). By combining temporal adjustments, ST is calculated from

$$ST = LST + 3.989(L_{ST} - L_{OB}) + E \tag{4}$$

where LST is local standard time, L_{ST} is standard meridian, L_{OB} is observed meridian, and E is equation of time.

Solar declination (δ) represents the earth's angular tilt to the sun, which shifts seasonally $\pm 23^\circ 26'$ between vernal and autumnal equinoxes (Duffie and Beckman, 1980). Declination is calculated using:

$$\delta = 23.439 \sin\left[360\left(\frac{283 + \text{Jday}}{365}\right)\right]. \tag{5}$$

The hour angle (ω) represents the angle of departure from solar noon (0°), which varies $\pm 15\ h^{-1}$, (i.e., positive east and negative west) and is used to correct for temporal deviations due to differences in longitude among sites, and seasonal differences that occur between LST and ST. Since ST is needed to accurately estimate solar coordinates, ω allows θ to be estimated:

$$\theta = \cos^{-1}(\sin\delta \sin\varphi + \cos\delta \cos\varphi \cos\omega), \tag{6}$$

where δ is declination angle, φ is observed latitude for the observed site, and ω is hour angle. For a more rigorous explanation of these predictive relationships refer to Forsythe et al. (1995), Mueller (1977), Rapp (1981), Stine and Harrigan (1985), and Campbell and Norman (1998).

2.3. Estimating photosynthetic photon flux density

Following effects from atmospheric light-attenuation, normal ground incidence GI_N is partitioned into sub-components, representing direct beam $GI_{DB} = GI_N\ (x)$ and diffuse incidence $GI_{DI} = GI_N\ (1 - x)$. The variable "x" is equivalent to a proportion of direct solar beam in relation to total solar incidence. The proportion of ground incidence ($x = GI_{DB}/GI_N$) received directly from direct solar beam is considered to be approximately 75% of the total solar flux (Monteith and Unsworth, 1990). Even though GI_{DB} is highly directional relative to GI_{DI} (downward angle across the skylight) total ground incidence (GI) can be estimated

$$GI = \cos\theta(GI_{DB} + GI_{DI}). \quad (7)$$

The temporal reference used for sunrise and sunset is a geometric definition based on the solar disc center perpendicular to normal ($\theta = 90^\circ$). Yet, unlike direct solar beam, atmospheric scattering of diffuse incidence is measurable prior to sunrise and sunset time. Therefore, the reference angle defined as civil twilight (CT) was used to regulate direct beam exposure. The CT occurs when the center of the sun is 6° below horizon and has approximately a 24 min time difference from geometric sunrise and sunset time. The temporal term initiating GI_{DB} is based on geometric sunrise and sunset ($\theta_{DB} = \theta$) (temporal differences due to refraction are not considered). However, to account for temporal differences among diffuse and direct incidence, we define onset and end time for GI_{DI} based on CT ($\theta_{DI} = \theta - 6^\circ$). Our relationship for estimating ground incidence does not differentiate between proportions of reflected albedo to reflected skylight.

At northern latitudes, the shortest radius vector (earth center to sun center) distance occurs during winter periods. Because of earth's asymmetric orbit, an adjustment to GI_N must be made to account for daily differences in solar distance (sd). This is expressed by:

$$sd = 1 + \cos\left[\left((Jday - 3)\frac{360}{365.2422}\right)0.0344\right] \quad (8)$$

where, 360 represents the earth's solar rotation, 365.2442 is number of days for an annual rotation, and ±3.44% is a distance offset. This results in a linear correction (astronomical units) to GI_N between 1.0344% on 3 January, to 0.9674% by 5 July (Thekaekara, 1977).

Although solar coordinates for the geometric center of sunrise and sunset can be derived, topographic relief is important when obstructive features vary in elevation along the solar ephemeris, as well as its influence on the proportion of visible skylight, here after referred to as viewshed (V_P). For this reason we estimated: (1) solar times for direct-rise and direct-set of the GI_{DB} for each Jday, (2) V_P and (3) canyon orientation. Topographic elevation angles were estimated using a geographical information system (GIS) hillshade function (ESRI, Inc., 2002) on a digital elevation model (DEM, 10 m cell size) for sites located on the CR centerline at 100 m intervals from Glen Canyon Dam to Pierce Ferry (Mietz and Gushue, 2002).

Diffuse incidence increases at angles adjacent to direct angular beam, and conversely decreases with greater zenith angles. Any decrease in viewshed reduces the quantity of diffuse incidence, even though the overall proportion may be small (≤25%) in relation to the direct solar beam (Monteith and Unsworth, 1990). Clearly, GI_{DI} is not evenly distributed across the V_P, although we assume that $V_P \approx GI_{DI}$. The total ground incidence is estimated by:

$$GI = [(\cos\theta_{DB} \times GI_{DB}) + (\cos\theta_{DI} \times GI_{DI} \times V_P)] \quad (9)$$

2.4. Topographic complexity

We used an arc-info routine referred to as hillshade function (ESRI, Inc., 2002) to generate binary grids, representing areas of shadow and illumination for a given set of azimuths and altitude angles. To avoid confusion, we distinguish between two types of altitude angles. Elevation angles (Ψ_E) refer to angles measured from a horizontal surface relative to a topographic feature, whereas illumination angles (Ψ_I) refer to the maximal angle between the topography and skyline. Ψ_I angles were sequentially searched incrementally over a

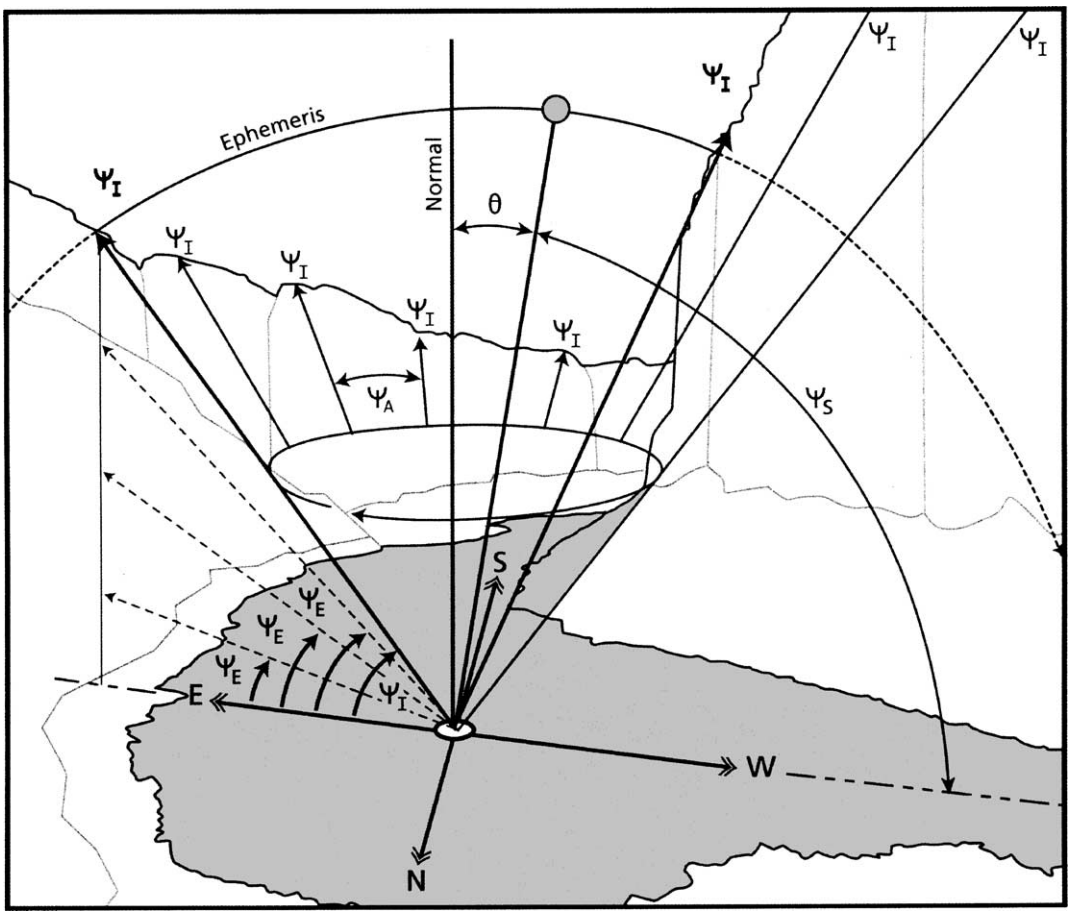

Fig. 2. A schematic, illustrating the major topographic and solar altitude angles used for estimating instantaneous total ground incidence (GI). Illustrated angles depicted are: zenith angle (θ) represents the angle between the sun and normal (N) a reference line perpendicular to the incidental water surface; elevation angle (Ψ_E) represents the angle measured from a horizontal surface relative to a topographic feature (i.e., angles are used to vertically search for illumination angle in single-degree increments); and illumination angles Ψ_I) are the maximum elevation angle between topographic skyline and horizon; solar altitude angle (Ψ_S) represent the angle between the sun and the horizon (i.e., Ψ_S angles are equivalent to $90^\circ - \theta$) along the ephemeris; and azimuth angles (Ψ_A) correspond to cardinal directions (N, E, S, and W) measured within the horizontal plane. Direct solar beam occurs when $\Psi_I \leq \Psi_S$, such that GI = [(cos θ_{DB} × GI_{DB}) + (cos θ_{DB} × GI_{DI} × V_P)] (refer to text).

360° azimuth circle. For every azimuth angle searched, a secondary loop was performed that advanced through the range (0–90°) of possible Ψ_E angles above the horizon. Every Ψ_E angle was assessed for illumination using a binary condition that iteratively advanced vertically at 1° increments. Once the condition for illumination occurred, the resulting angle represented the altitude of the topographic skyline (Fig. 2). For all possible azimuth angles, 360 Ψ_I angles were calculated repetitively at 0.1 km increments along the river's centerline for over 4745 sites.

Although for a given site there were a total of 360 Ψ_I angles, only two of these Ψ_I angles (east and west meridian) for a particular day achieved congruence with the altitude angle of the sun (Ψ_S). These congruent angles represented the topographic point where ground incidence shifted daily from diffuse to direct beam, and back again from direct beam to diffuse conditions. Solar altitude angle (Ψ_S) corresponds to the θ angle, such that a Ψ_S angle is equivalent to $90^\circ - \theta$. We used a computational routine that initiated a search based on the estimated geometric sunrise and sunset time for a

particular day. For every day, topographic direct-rise and direct-set times were determined by sequentially comparing all Ψ_I (direct rise and set) to known Ψ_S angles found within the solar ephemeris. This routine was performed in 1 min time increments until the congruent condition $\Psi_I \geq \Psi_S$ occurred. Resulting Ψ_I angle represented the angular location and solar time when topography no longer obstructed direct solar beam. All estimated times for direct solar beam were site dependent and varied daily due to changes in observed latitude, declination, and topographic relief; and based on this temporal condition the term $(\cos\theta_{DB} \cdot GI_{DB})$ was either used or excluded from Eq. (9).

Proportional area of the viewshed (V_P) was determined using analytical geometry (Anton, 1984), where for each azimuth angle (i), arc- or sky angle (α_i) was determined from the corresponding Ψ_{Ii} angle to normal ($\alpha_i = 90^\circ - \Psi_{Ii}$), such that the total proportion of visible sky was described by:

$$V_P = \left(\frac{\sum_{i=1}^{360} \alpha_i / 90}{360} \right). \quad (10)$$

Only one of four possible channel orientations is assigned to each site, these cardinal directions included: north–south (NS), northwest–southeast (NW–SE), east–west (EW), and northeast–southwest (NE–SW). Channel orientation was determined for each site using a routine that searched all possible azimuth angles and selected a discrete cardinal direction based on the lowest Ψ_I angles encountered in the V_P. Ortho-rectified photos were used to validate method for estimating channel orientation.

Empirical data for PPFD ($\mu mol\, m^{-2}\, s^{-1}$) were adjusted to normal by accounting for differences attributed to θ (Eq. (6)) and solar distance (Eq. (8)). We estimated the parameter GI_N (Eq. (9)) by regressing observed against estimated incidence and solved for the best fit. Daily solar insolation estimates were derived using a numerical solution that estimated instantaneous PPFD through summation over discrete time steps (1 min intervals). We chose this approach over other methods because our purpose was to develop a method for estimating aquatic primary production in an optically and hydrologically variable environment using a discrete-state modeling approach that required instantaneous PPFD estimates at smaller time increments (Yard, 2003). Although, our approach lacks an elegant integration of insolation, it allows us to dynamically control for other environmental variables operating at smaller time increments.

2.5. Statistical analysis

Main effects ANOVA (Type VI unique) was used to test for seasonal mean differences and interactions of daily solar insolation among canyon sections, geomorphic reaches, and channel orientation (Sokal and Rohlf, 1995). Multiple comparison procedures (Single-factor ANOVA and Tukey unequal NHSD) were used as post hoc tests to determine group mean differences. Simple linear regressions and bootstrap techniques were used to compare differences among observed and predicted estimates of GI_N (Neter et al., 1996). We determined relative error in our modeled estimates from atmospheric influence under clear or cloudy conditions. Using a bootstrap technique, observed data for a range of varying atmospheric conditions were analyzed to determine relative error ($RE = (E - O)/O$) representing the estimated error (E) relative to an observed measurement (O). Data used for this analysis were independent from data previously used for estimating parameter GI_N. Data were segregated, representing either clear skies or cloudy conditions. For each resample, 500 random samples were selected from empirical data for clear skies (n = 29,813) cloudy skies (n = 25,051), and intermittent clouds (n = 9275). Median RE was iteratively sampled with replacement for 10,000 bootstrap samples. Multiple statistical packages were used (Statistica Statsoft, Inc., 1997; Resampling Stats, Inc., 2001).

3. Results

Our estimated GI_N was $2326\, \mu mol\, m^{-2}\, s^{-1}$ ($r^2 = 0.94$, $n = 4312$, S.E. $\pm$ 36.3) that represented clear-sunny daytime conditions characteristic of this large geographical region. Observed data used for estimating this parameter varied from 1321–2063 $\mu mol\, m^{-2}\, s^{-1}$, and included zenith angles from 12.79°–49.79°. Solar distance adjustment to GI_N varied linearly $2326 \pm 80\, \mu mol\, m^{-2}\, s^{-1}$ over a 182.5 days period (Eq. (8)).

3.1. Relative error in estimation of instantaneous incidence

Data were collected over a range of field conditions, and different years (1992–2001), seasons, and times and sites. Instantaneous PPFD averaged 1052 μmol m^{-2} s^{-1} and varied between 0.15 and 2100 μmol m^{-2} s^{-1}. Although a strong correlation ($p < 0.001$, $r^2 = 0.987$, $n = 58{,}060$) existed among observed and estimated data, variation in solar incidence increased during periods of continuous or intermittent cloud cover. Our median RE for observed incidence under clear skies for all seasons was 2.3%, with a 95% bootstrap confidence interval ($CI_{95\%}$) of 1.85–2.75%; whereas, under cloudy conditions median RE was 100%, with a $CI_{95\%}$ of 92.5–107.5%. RE was most pronounced during late-July through September monsoons, and winter (December–March) when cloud cover was greatest. However, an inverse response occurred during intermittent cloud cover, which had an estimated incidence less than observed (−2%), and had a $CI_{95\%}$ of −1.8 to −2.2%. This heightened response was perhaps due to enhanced atmospheric scattering (Kirk, 1983).

We used a continuous set of logged PPFD measurements (1992–1993), averaged over a 10 min period to compare differences among observed and estimated daily solar insolation (mol m^{-2} d^{-1}). Under optimal atmospheric conditions, results corresponded linearly among estimated and observed daily insolation ($r^2 = 0.987$, S.E. ± 9.3, Fig. 3).

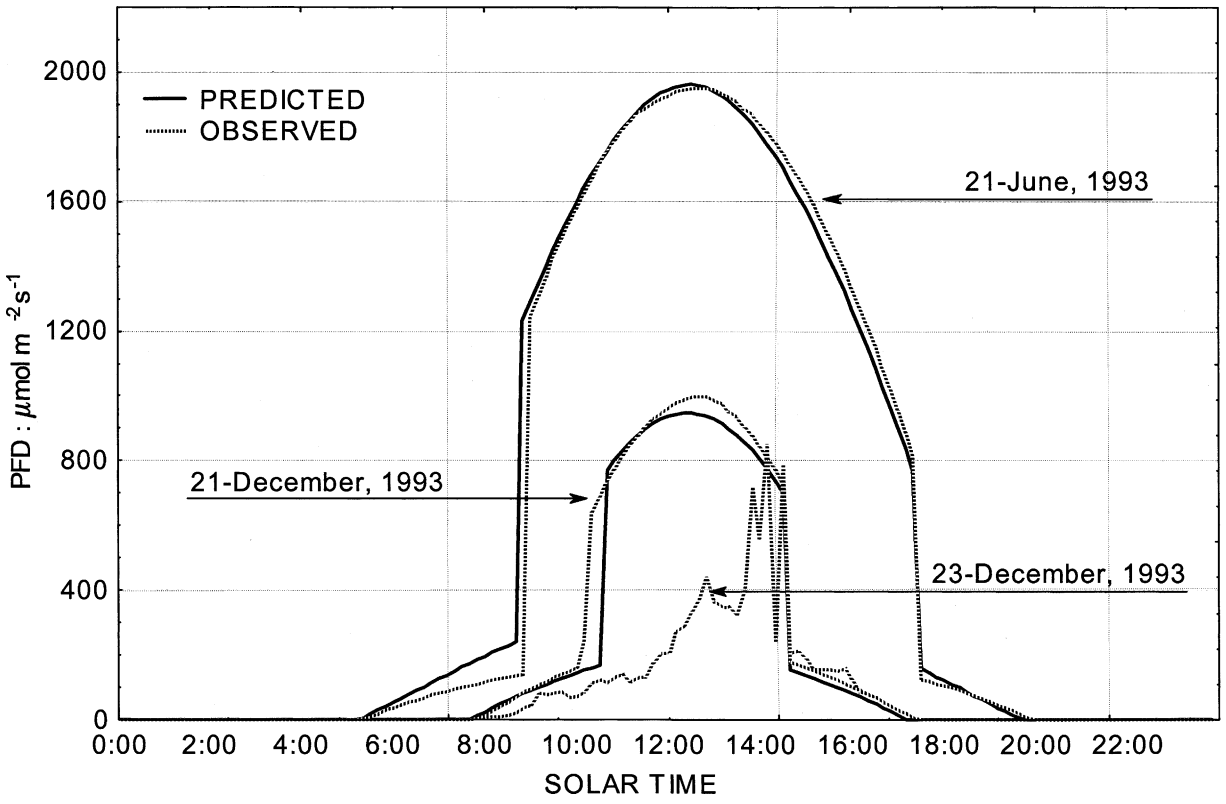

Fig. 3. Predicted and observed daily solar insolation estimates (mol quanta m^{-2} d^{-1}) for summer (22 June 1992) and winter (21 December 1993). Observation site was located 76.5 km downstream in Marble Canyon Gorge (36°12′6.6″N, 111°48′0.3″W) having a north-south channel orientation. Data collected on 23 December 1992 demonstrates the influence atmospheric interference has on mean daily solar insolation relative to the estimate.

3.2. System wide comparisons among topographic and idealized conditions

At an ecosystem-scale, annual estimates of average daily insolation for topographically complex environments differed considerably when compared to idealized conditions (no topographic relief: $\Psi_E = 0^\circ$ and $V_P = 1.0$) (Tables 2 and 3). Under idealized conditions, mean annual daily insolation levels for CR was estimated at 52.3 mol m^{-2} d^{-1} (15.7 S.D.). Alternately, when taking into account topographic interference, mean annual daily insolation was 36.0 mol m^{-2} d^{-1} (17.5 S.D.) for all sites (Table 2). Differences in mean daily insolation due to topographic relief varied seasonally, and on average were reduced from ideal by 22% during summer, and as much as 53% during winter. Comparisons among ideal and topographically complex environments demonstrate that varying physical obstructions strongly influence the seasonal quantity of solar insolation reaching the CR corridor.

For idealized day-length estimates for geometric sunrise to sunset ranged seasonally from 568–872 min; however, when topographic complexity was taken into account, total day-length for direct beam varied seasonally within and among the different canyon sections, geomorphic reaches, and channel orientations, and day length estimates for direct beam were considerably less. Mean direct beam day-length for entire CR system averaging 369 min (184 S.D.) annually, and varied seasonally among summer (551 min; 108 S.D.) and winter (161 min; 126 S.D.).

3.3. Canyon sections, geomorphology and channel orientation

Canyon sections, geomorphic reaches, and channel orientation significantly interacted to influence solar insolation levels measured at sites ($n = 4745$) for summer ($F_{54,694} = 3.82$, $p < 0.01$) and winter ($F_{54,694} = 5.41$, $p < 0.01$), and yet had no main factor effects or intermediate interactions (Tables 2 and 3). Analyzed separately, post hoc tests (one-way ANOVA) revealed significant differences between each of the single factors. Seasonal variation in solar insolation was significantly different for canyon sections during both summer ($F_{34,741} = 310$, $p < 0.01$) and winter ($F_{34,741} = 18$, $p < 0.01$) (Table 3), geomorphic reaches during both summer ($F_{124,732} = 208$, $p < 0.01$) and winter ($F_{124,732} = 171$, $p < 0.01$), and channel orientation for summer ($F_{34,741} = 328$, $p < 0.01$) and winter ($F_{34,741} = 668$, $p < 0.01$) (Table 3).

Topographic relief reduced viewshed (V_P), as well as duration of direct solar exposure. For all sites evaluated, V_P ranged from 0.45 to 0.95. Canyon sections and geomorphic reaches having the highest Ψ_I angles and smallest V_P were: Marble Canyon Section (Supai Gorge, 43.5–61.7 km; Redwall Gorge, 61.7–83.1 km; and Lower Marble Canyon, 83.1–124.3 km), and Western Grand Canyon Section (Muav Gorge, 250.5–282.7 km) (Fig. 1). Differences in Ψ_I angles and predominant channel orientation varied among different geomorphic reaches and canyon sections. Mean Ψ_I angles for all sites in the CR ecosystem (475 km) ranged from 12.6° to 47.4° and averaged 33.9° (4.43 S.D.) (Table 2). Canyon sections and geomorphic reaches influenced the geographical distribution and variability of Ψ_I angles within and among sites, of these angles, and the sequence of repetitive patterns occurring system-wide (Fig. 4).

Average annual insolation levels were not significantly different among channel orientations. NS orientation averaged 35.97 mol m^{-2} d^{-1} (14.1 S.D., $n = 461{,}892$) and EW was 35.96 mol m^{-2} d^{-1} (21.7 S.D., $n = 418{,}338$). Depending on outlying topography in canyon bound regions; NS orientations exhibited far less variation in daily insolation among seasons than did EW (Table 3, Figs. 4 and 5). Summer solar insolation for EW orientations was significantly higher ($p < 0.01$, HSD) than that of NS. Conversely, during winter EW orientations received significantly less solar insolation ($p < 0.01$, HSD) than NS.

Under idealized conditions (lacking topographic effect) summer and winter estimates for mean daily insolation were 73.2 and 28.4 mol m^{-2} d^{-1}. In comparison, summer and winter estimates for mean daily insolation for NS orientation was 52.7 and 17.7 mol m^{-2} d^{-1}, respectively; whereas, EW orientation was 61.4 and 8.1 mol m^{-2} d^{-1}, respectively. This winter difference due to orientation is considerable, especially with respect to EW orientation where mean daily insolation levels were on average reduced to 72% from ideal (Table 3).

Direct incidence was topographically obstructed during part of the year for 70% of mid-channel sites having EW orientation and of these sites, average diffuse light conditions persisted for 19.3% of the year

Table 2
Annual and seasonal (21 June and 21 December) estimates of mean daily solar insolation levels (mol quanta m^{-2} d^{-1}) for major canyon sections and geomorphic reaches in Colorado River from Glen Canyon Dam to Grand Wash Cliffs, Lake Mead, AZ

Major Canyon sections geomorphic reaches	Channel surface area (ha)	Mean ψ_E (S.D.)	Illumination angle		Mean V_p (S.D.)	Mean annual, mol m^{-2} d^{-1} (S.D.)	Mean winter, mol m^{-2} d^{-1} (S.D.)	Mean summer, mol m^{-2} d^{-1} (S.D.)	Minimum (mol m^{-2} d^{-1})	Maximum (mol m^{-2} d^{-1})	Sites
			Minimum (ψ_I)	Maximum (ψ_I)							
Glen Canyon	321.6	31.3° (14.2)	3°	70°	0.65 (0.07)	35.2 (18.3)	11.7 (6.1)	57.0 (6.8)	4.6	69.0	268
Marble Canyon	743.0	35.4° (12.5)	4°	71°	0.61 (0.07)	32.2 (15.4)	12.5 (4.8)	50.9 (7.3)	4.0	68.3	975
Permian section	156.3	30.1° (13.4)	4°	56°	0.68 (0.06)	36.6 (15.4)	15.2 (4.2)	55.9 (6.0)	5.8	68.3	167
Supai gorge	103.1	37.7° (11.0)	10°	54°	0.61 (0.03)	31.8 (14.6)	12.3 (4.4)	50.3 (6.3)	5.0	64.3	182
Redwall gorge	130.9	37.5° (11.4)	11°	53°	0.59 (0.06)	30.6 (14.9)	11.2 (3.7)	48.7 (7.2)	4.6	62.4	214
Lower marble Canyon	386.2	35.5° (12.8)	5°	71°	0.59 (0.06)	31.5 (15.6)	12.2 (5.4)	50.2 (7.1)	4.0	61.9	412
Central Grand Canyon	886.8	34.2° (13.0)	6°	65°	0.68 (0.06)	37.9 (17.9)	13.3 (6.5)	59.2 (5.3)	4.4	68.7	1262
Furnace flats	256.8	36.6° (12.5)	11°	55°	0.75 (0.07)	42.1 (16.0)	19.8 (5.6)	61.6 (5.8)	5.6	68.7	256
Upper granite gorge	360.8	35.2° (13.2)	7°	65°	0.65 (0.05)	35.9 (18.7)	10.2 (5.6)	58.1 (5.4)	4.4	65.8	650
Aisles	76.4	29.3° (10.7)	6°	55°	0.67 (0.01)	38.0 (17.0)	13.7 (4.9)	58.5 (5.1)	5.8	64.4	124
Middle granite gorge	125.9	31.5° (12.9)	6°	60°	0.69 (0.03)	38.8 (17.2)	14.2 (5.1)	60.2 (3.2)	5.6	64.8	232
Western Grand Canyon	1562	34.7° (14.8)	8°	69°	0.66 (0.10)	36.7 (17.8)	14.0 (7.0)	57.6 (7.3)	4.1	71.7	2240
Muav gorge	170.4	36.7° (14.4)	11°	66°	0.53 (0.03)	27.2 (17.8)	7.0 (3.1)	48.6 (9.5)	4.1	63.2	322
Lower Canyon	662.5	36.0° (14.8)	8°	69°	0.64 (0.09)	35.0 (18.0)	12.1 (6.5)	56.8 (6.4)	4.2	67.0	867
Lower granite gorge	142.5	32.4° (15.2)	8°	59°	0.70 (0.05)	39.4 (17.0)	15.2 (6.4)	60.0 (4.0)	5.1	65.7	518
Western Canyon	586.3	30.8° (13.8)	8°	54°	0.75 (0.05)	42.6 (15.3)	20.1 (4.1)	61.9 (4.2)	6.3	71.7	533
Colorado River ecosystem	3721	33.9° (13.8)	3°	71°	0.66 (0.09)	36.0 (17.5)	13.4 (6.5)	57.4 (6.8)	4.0	71.7	4745

Water surface area (ha) derived from STARS simulation model (Randle and Pemberton, 1987) based on Colorado River mean annual discharge of 323 m^{-3} s^{-1}. Mean illumination angles (ψ_I) expressed in degrees, and derived from 10 m GIS coverage using arc-info hillshade routine (ESRI, Inc., 2002) (n = site × 360). Solar insolation levels were calculated along river centerline at hectometers for total year (n = site × 366 days) and season (summer and winter solstice; n = site × days).

Table 3
Summary data of mean daily insolation levels (mol m^{-1} d^{-1}) have been estimated for summer and winter seasons (21 June and 21 December) for the primary channel orientations, north–south (NS), northwest–southeast (NW–SE), east–west (EW), and northeast–southwest (NE–SW), and distributed within the different canyon sections and geomorphic reaches of the Colorado River (total distance of 474.5 km from Glen Canyon Dam to Grand Wash Cliffs, Lake Mead, AZ)

	NS-orientation, mol m^{-2} d^{-1} (S.D., *n*)		EW-orientation, mol m^{-2} d^{-1} (S.D., *n*)		NW–SE-orientation, mol m^{-2} d^{-1} (S.D., *n*)		NE–SW-orientation, mol m^{-2} d^{-1} (S.D., *n*)	
	Summer	Winter	Summer	Winter	Summer	Winter	Summer	Winter
GC	50.5 (5.4)	15.6 (3.3, *n* = 41)	61.2 (2.9)	8.4 (5.0, *n* = 91)	55.6 (6.3)	15.5 (6.1, *n* = 71)	56.5 (7.2)	9.2 (4.7, *n* = 65)
MC	47.3 (6.8)	15.1 (3.3, *n* = 349)	58.1 (3.5)	5.5 (2.3, *n* = 96)	49.6 (6.1)	14.1 (3.9, *n* = 160)	52.9 (6.8)	11.3 (4.7, *n* = 370)
PS	53.1 (5.2)	17.4 (2.6, *n* = 54)	66.8 (0.5)	11.2 (6.3, *n* = 4)	–	–	56.9 (5.8)	14.3 (4.3, *n* = 109)
SG	47.0 (4.1)	14.8 (2.3, *n* = 109)	61.2 (1.3)	13.6 (0.7, *n* = 3)	–	–	55.0 (5.7)	8.3 (4.1, *n* = 69)
RG	41.6 (5.5)	12.6 (2.4, *n* = 40)	57.2 (2.7)	4.8 (0.1, *n* = 12)	40.0 (7.8)	8.8 (2.3, *n* = 20)	51.2 (5.8)	11.7 (3.7, *n* = 142)
LMC	46.9 (7.6)	15.1 (3.8, *n* = 146)	57.7 (3.1)	5.0 (0.8, *n* = 77)	51.0 (4.5)	14.9 (3.5, *n* = 139)	46.0 (6.0)	7.8 (3.9, *n* = 50)
CGC	55.4 (5.4)	18.6 (3.2, *n* = 278)	62.9 (2.1)	8.3 (4.5, *n* = 385)	57.0 (4.9)	12.9 (6.1, *n* = 322)	60.6 (4.7)	15.6 (6.5, *n* = 277)
FF	58.8 (5.7)	20.7 (3.5, *n* = 108)	65.0 (2.4)	13.0 (7.4, *n* = 31)	58.3 (4.5)	23.8 (1.1, *n* = 6)	63.6 (5.3)	20.7 (5.6, *n* = 111)
UGG	52.5 (4.4)	16.6 (2.3, *n*= 107)	62.4 (2.2)	7.3 (3.7, *n* = 252)	55.7 (5.0)	11.3 (5.8, *n* = 232)	59.6 (2.5)	8.4 (3.3, *n* = 59)
AI	53.1 (2.1)	17.7 (0.8, *n* = 44)	63.5 (1.0)	9.4 (4.2, *n* = 55)	58.4 (2.2)	17.1 (2.2, *n*= 16)	54.1 (2.0)	14.4 (1.7, *n* = 9)
MGG	57.5 (2.4)	19.3 (1.1, *n* = 19)	63.7 (1.1)	9.0 (4.3, *n* = 47)	60.9 (2.4)	16.3 (5.6, *n* = 68)	58.4 (2.8)	14.3 (3.8, *n* = 98)
WGC	54.9 (9.0)	18.9 (4.4, *n* = 594)	60.8 (4.1)	8.3 (5.7, *n* = 571)	59.5 (5.0)	16.7 (5.6, *n* = 480)	55.6 (7.9)	12.2 (6.8, *n* = 595)
MG	37.4 (4.0)	10.7 (2.1, *n* = 93)	57.8 (2.9)	4.9 (1.0, *n* = 119)	48.6 (6.1)	4.6 (0.5, *n* = 21)	48.2 (6.6)	6.5 (2.6, *n* = 89)
LC	54.9 (5.7)	18.6 (3.0, *n* = 175)	59.6 (4.0)	7.4 (4.8, *n* = 256)	61.8 (4.9)	19.0 (5.7, *n* = 78)	54.5 (6.9)	10.6 (5.1, *n* = 358)
LGG	60.1 (4.4)	21.7 (2.2, *n* = 124)	62.8 (1.3)	7.2 (2.6, *n* = 111)	57.9 (4.3)	14.2 (4.9, *n* = 172)	60.5 (2.8)	17.5 (4.8, *n*= 111)
WC	59.7 (3.0)	21.2 (1.8, *n* = 202)	65.8 (1.3)	17.4 (5.6, *n* = 85)	61.0 (3.3)	19.1 (3.4, *n* = 209)	69.6 (3.0)	25.7 (5.4, *n* = 37)
CR	52.7 (8.4)	17.7 (4.2, *n* = 1,262)	61.4 (3.7)	8.1 (5.1, *n* = l,143)	56.9 (6.2)	15.0 (5.8, *n* = 1,033)	55.9 (7.4)	12.6 (6.3, *n* = 1307)

The standard deviation (S.D.) and site frequency (n) are indicated.

(70.5 days). Some sites were exposed solely to diffuse conditions upwards of 194 days. Conditions of diffuse incidence were most prevalent in Redwall Gorge and Muav Gorge, where sites averaged 130 days of diffuse incidence (Figs. 4 and 5). In contrast, NS oriented sites that were exposed to only diffuse incidence occurred less than 0.1% of the time and only during winter. Because of declinational shift during winter season (3 months), mid-day maximum PPFD levels are 900–1100 μmol m^{-2} s^{-1} (i.e., winter maximum solar altitude Ψ_I at solar noon varied from 30° to 40°). Duration of diffuse incidence is prevalent system-wide especially for EW orientation because of the higher southerly skyline angles (Ψ_I angles 33.9°, 13.8 S.D.) that often exceeded the maximum daily solar altitude angle (Ψ_S) (Fig. 4).

Daily insolation was greatly reduced for most sites in winter. Sites having EW orientations, exposed solely to diffuse incidence from October through March, had daily mean instantaneous PPFD levels from 80 to 170 μmol m^{-2} s^{-1}, with maximum mid-day intensities from 125 to 300 μmol m^{-2} s^{-1}. In contrast, sites having NS orientation with direct exposure had daily mean instantaneous PPFD levels from 490 to 810 μmol m^{-2} s^{-1}, with maximum mid-day intensities from 950 to 1725 μmol m^{-2} s^{-1}. Other orientations (NW–SE and NE–SW) were intermediate to these more extreme canyon orientations (Table 3).

4. Discussion

Localized topography strongly affected availability of daily solar insolation levels received at Colorado River surface (Figs. 4 and 5). At a system-wide scale, topographic complexity generates a spatial and temporal mosaic of varying solar insolation. This variation was a predictable consequence of canyon orientation, elevation angles and viewshed. Canyon sections and geomorphic reaches receiving greatest quantity of solar insolation were located in areas having lowest Ψ_I angles and largest V_P (Fig. 1, Table 2). These same canyon sections and reaches were either adjacent to major tributaries or in the lower canyon sections.

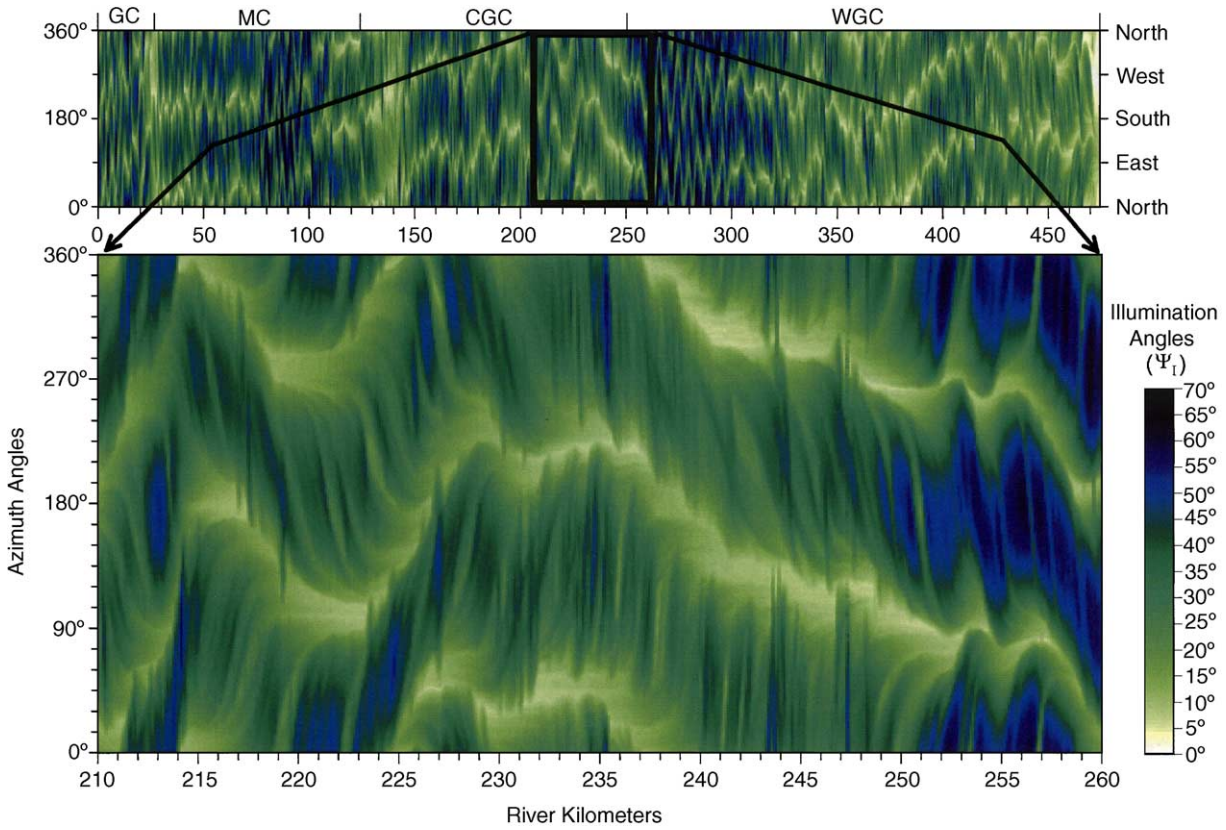

Fig. 4. Graphical results generated from GIS coverage using Arc-Info Hillshade routine (ESRI, Inc., 2002) for illumination angles (Ψ_I, degrees) measured over the cardinal directions, (i.e., north, east, south and west) (*y*-axis, 360° azimuth) along the center-line at every hectometer for the entire river length (*x*-axis) from Glen Canyon Dam to Lake Mead (474.5 km). The lower graph represents a more resolute subset of Ψ_I distributed over a 360° azimuth circle from 210 km to 260 km. Major canyon sections indicated are: Glen Canyon (GC), Marble Canyon (MC), Central Grand Canyon (CGC), and Western Grand Canyon (WGC).

Topographic relief may influence distribution, biomass, and composition of phytobenthic community, as well as seasonal primary production levels occurring in this system. Suspended-sediment loads are responsible for underwater light-attenuation due to sediment-supply and transport processes (Rubin and Topping, 2001). We hypothesize that if the phytobenthic community is seasonally light-limited in the CR as indicated by Stevens et al. (1997a) its vertical extent and spatial distribution may be regulated not only by apparent optical properties of water (i.e., normal light-attenuation coefficients, $K_N > 0.8$) (Yard, 2003), but also by the initial quantity of solar insolation available at water surface. Spatio/temporal differences in solar incidence are strongly regulated by topographic relief, yet remain independent of other factors that attenuate underwater light or preclude phytobenthic colonization.

Turbidity has been recognized as increasing with downstream distance (Hardwick et al., 1992; Shaver et al., 1997; Stevens et al., 1997a). Suspended-sediment has a strong influence on the distributional patterns (biomass/density) of primary and secondary benthos (Shaver et al., 1997; Stevens et al., 1997a; Wilson et al., 1999), fish (Schmidt et al., 1998), waterfowl and piscivorous raptors in this system (Stevens et al., 1997b). Also, geomorphology has significant secondary effects on aquatic and aquatically linked biota in the canyon (Stevens et al., 1997a, 1997b). The vertical distribution of the phytobenthic community is likely to adjust in response to seasonal light-depth limitations. Persistence

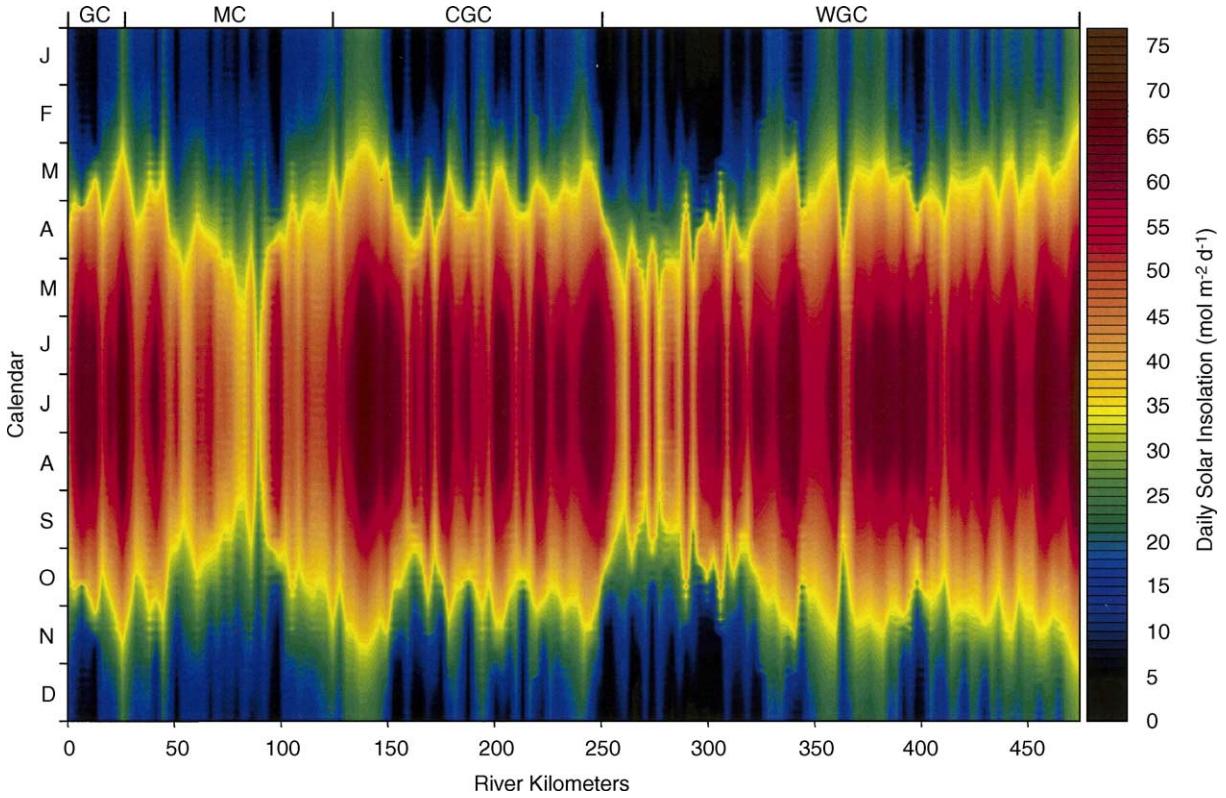

Fig. 5. Planar view represents the spatial and temporal distribution of maximum daily solar insolation (mol quanta m^{-2} d^{-1}) for the entire year (*y*-axis) along the entire river length (*x*-axis) in kilometers from Glen Canyon Dam to Lake Mead (474.5 km). Major canyon sections indicated are: Glen Canyon (GC), Marble Canyon (MC), Central Grand Canyon (CGC), and Western Grand Canyon (WGC).

and/or reestablishment at or below compensation point levels for the phytobenthic community require either different physiological and metabolic pathways (Blum, 1956; Whitton, 1970; Dudley and D'Antonio, 1991) or colonization mechanisms (Whitton, 1970). Algal colonization rates in this dam-regulated system are slow (>6 months) (Shaver et al., 1997; Benenati et al., 1998) and occur primarily by fragmentation. This is attributed to cold stenothermic conditions (Shannon et al., 1994; Shaver et al., 1997; Blinn et al., 1998).

For this system, cross-channel variation is small for NS channel orientation because daily insolation levels are regulated by differences in elevation angles along the east and west canyon rims. Generally, these angles vary little along the solar ephemeris. Alternately, EW channel orientations demonstrate greater cross-channel variation between southern and northern banks. This variation is greatest during winter. We hypothesize that light-depth limitation should be most evident for EW oriented channels having high elevation angles, and expect to observe decreased primary production during winter, and alternately higher production and standing biomass during summer periods when channel receives considerably more solar incidence. There is some evidence for this phytobenthic pattern; however, the vertical distribution is further compounded by longitudinal differences in optical properties throughout the CR.

Owing to the increased duration of diffuse light conditions during winter, it is hypothesized that deeper benthic establishment and persistence is likely to be precluded (Yard, 2003). The reasons for this are: (1) winter maximum daily diffuse incidence at water surface was estimated at 250–300 μmol m^{-2} s^{-1}, and is considered below onset of light saturation for *Cladophora glomerata* (Graham et al., 1982); (2) depth

distribution of algae persisting at or above metabolic maintenance may be limited solely to the varial zone because PPFD decreases exponentially as a function of depth (Blinn et al., 1995); (3) algal growth in this zone is susceptible to diel flow fluctuations and desiccation (Blinn et al., 1995; Shaver et al., 1997; Stevens et al., 1997a) and (4) solar insolation estimates are overestimated during winter due to increased atmospheric interference.

We demonstrate that topographic relief affects daily and seasonal solar incidence in different canyon sections and geomorphic reaches; and hypothesize that system-wide primary production varies spatially and temporally (Figs. 4 and 5). Secondly, we argue that the phytobenthic response is regulated by solar insolation, colonization constraints, underwater light-attenuation, and desiccation by regulated flow fluctuations (Blinn et al., 1995; Shaver et al., 1997; Worm et al., 2001, Yard, 2003). Additionally, solar insolation has broader ecological implications to the CR ecosystem. Patterns of daily solar insolation correspond to total radiation transmission, and probably explain some of the distribution and phenology of xeric and riparian vegetation in the deep canyon ecosystem (Clover and Jotter, 1994; Jones, 1992; Evett et al., 1994; Stevens et al., 1995). Findings suggest that future comparisons made among different regulating mechanisms (turbidity and geomorphology) should also include temporal variation in solar insolation, as both local and canyon-wide geomorphology, and canyon orientation are intercorrelated with seasonal differences in solar insolation.

5. Conclusion

Determining the availability of daily, seasonal and annual solar insolation levels should be considered when characterizing aquatic primary production, especially in topographically complex riverine environments. The approach we used is one such method, and provides an effective means to quantify spatio/temporal variability of incoming solar insolation. However, relative error for instantaneous values among observed and predicted demonstrates model overestimation due to atmospheric interference. Although this method departs from observed, it provides an estimate for a maximum limit within or among different spatial and temporal scales. Because climate often lacks deterministic qualities, developing estimates having greater accuracy and precision across all scales should be objective based. Although problematic, it is resolvable empirically using remote sensors with appropriate density and distribution.

We developed a computational program that numerically solves for solar time, spatial coordinates and solar insolation so that other researchers may resolve similar questions in this and other topographically complex systems. The solar insolation model was written in Visual Basic for applications (Microsoft Visual Basic, 1999), with several subroutines designed for an Excel worksheet environment (Microsoft Excel, 2000). Documentation, downloading, and page access to updates are available at: http://www.gcmrc.gov.

We recommend that users determine whether or not our estimated GI_N is an appropriate estimate for their locality, partly because transmissivity differences may require adjustments to GI_N. Additionally, the model does not account for subtle differences in solar incidence when the ephemeris follows the topographic skyline and/or multiple topographic direct-rise and direct-set times during a single day. Even though altitude angles at specific sites were determined using 10 m DEM in a GIS-environment, other alternate methods are just as practical for geo-referencing and calculating elevation angles. Technological methods range from conventional surveying to handheld protractors.

Acknowledgements

Geographic data presented in this paper were collected and analyzed by Grand Canyon Monitoring and Research Center at US Geological Survey. Partial research funding was obtained from a cooperative agreement 98-FC-40-0540 to Northern Arizona University. We appreciate the editorial assistance from two anonymous reviewers. Also, thanks and appreciation are extended to D. Baker, B. Gold, T. Gushue, G.A. Haden, B. Hungate, G. Koch, A. Martinez, D. McKinnon, R. Parnell, P. Price, B. Ralston, S. Wyse, M. Williams, and many others who assisted and supported certain aspects of this study, and the National Park Service at Glen Canyon National Recreational Area and Grand Canyon National Park.

References

Anton, H., 1984. Calculus with Analytical Geometry, second ed. John Wiley and Sons, New York, NY.

Benenati, P.L., Shannon, J.P., Blinn, D.W., 1998. Desiccation and recolonization of phytobenthos in a regulated desert river: Colorado River at Lees Ferry, Arizona, USA. Regul. Riv. 14, 519–532.

Benenati, P.E., Shannon, J.P., Blinn, D.W., Wilson, K.P., Hueftle, S.J., 2000. Reservoir–river linkages: Lake Powell and the Colorado River, Arizona. J. N. Am. Benthol. Soc. 19, 742–755.

Blinn, D.W., Cole, G.A., 1991. Algal and invertebrate biota in the Colorado River: comparison of pre- and post-dam conditions. In: Marzolf, G.R. (Ed.), Colorado River Ecology and Dam Management: Proceedings of a Symposium. National Academy Press, Washington, DC, pp. 102–123.

Blinn, D.W., Shannon, J.P., Stevens, L.E., Carver, J.P., 1995. Consequences of fluctuating discharge for lotic communities. J. N. Am. Benthol. Soc. 14, 233–248.

Blinn, D.W., Shannon, J.P., Benenati, P.L., Wilson, K.P., 1998. Algal ecology in tailwater stream communities: the Colorado River below Glen Canyon Dam, Arizona. J. Phycol. 34, 734–740.

Blum, J.L., 1956. The ecology of river algae. Bot. Rev. 22, 291–341.

Campbell, G.S., Norman, J.M., 1998. An Introduction to Environmental Biophysics, second ed. Springer-Verlag, New York.

Clover, E., Jotter, L., 1994. Floristic studies in the canyon of the Colorado and tributaries. Am. Midl. Nat. 32, 591–642.

Cole, G.A., 1983. Textbook of limnology, third ed. Waveland Press, Inc., Prospect Heights, IL.

Cousins, F.W., 1969. Sundials: A Simplified Approach by Means of the Equatorial Dial. John Baker Publishers, London.

Dozier, J., Frew, J., 1990. Rapid calculation of terrain parameters for radiation modeling from digital elevation data. IEEE Trans. Geosci. Remote Sens. 28, 963–969.

Dozier, J., Outclat, S.I., 1979. An approach toward energy balance simulation over rugged terrain. Geogr. Anal. 11, 65–85.

Dubayah, R., Rich, P.M., 1995. Topographic solar radiation models for GIS. Int. J. Geogr. Infor. Syst. 9, 405–413.

Dudley, T.L., D'Antonio, C.M., 1991. The effects of substrate texture, grazing and disturbance on macroalgal establishment in streams. Ecology 72, 297–309.

Duffie, J.A., Beckman, W.A., 1980. Solar Engineering of Thermal Processes. John Wiley and Sons, New York, NY.

Environmental Systems Research Institute, Inc., 2002. ARC/INFO Version 8.21. Redlands, CA, USA.

ESRI, Inc., 2002. Environmental Systems Research Institute, Inc., ARC/INFO Version 8.21. Redlands, CA, USA.

Evett, S.R., Warrick, A.W., Matthias, A.D., 1994. Energy balance model of spatially variable evaporation from bare soil. Soil. Sci. Soc. Am. J. 58, 1604–1611.

Forsythe, W.C., Rykiel Jr., E.J., Stahl, R.S., Wu, H., Schoolfield, R.M., 1995. A model comparison for daylength as a function of latitude and day of year. Ecol. Model. 80, 87–95.

Frontline Systems, Inc., 1999. NLP/NSP Solver DLL Version 3.5. Incline Village, NV.

Graham, J.M., Auer, M.T., Canale, R.P., Hoffman, J.P., 1982. Ecological studies and mathematical modeling of *Cladophora* in Lake Huron: 4. Photosynthesis and respiration as functions of light and temperature. J. Great Lakes Res. 8, 100–111.

Gregory, S.V., Swanson, F.J., McKee, W.A., Cummins, K.W., 1991. An ecosystem perspective of riparian zones, focus on links between land and water. Bioscience 41, 540–551.

Haden, G.A., Blinn, D.W., Shannon, J.P., Wilson, K.P., 1999. Driftwood: an alternative habitat for macroinvertebrates in a large desert river. Hydrobiologia 397, 179–186.

Hardwick, C.G., Blinn, D.W., Usher, H.D., 1992. Epiphytic diatoms on *Cladophora glomerata* in the Colorado River, Arizona: longitudinal and vertical distribution in a regulated river. Southwestern Naturalist 37, 17–30.

Hawkins, C.P., Murphy, M.L., Anderson, N.H., 1982. Effects of canopy, substrate composition, and gradient on the structure of macroinvertebrate communities in Cascade Range streams of Oregon. Ecology 63, 1840–1856.

Hill, W., 1996. Factors affecting benthic algae. Effects of light. In: Stevenson, R.J., Bothwell, M.I., Lowe, R.L. (Eds.), Algal Ecology: Freshwater Benthic Ecosystems. Academic Press, Inc., San Diego, CA, pp. 121–144.

Howard, A., Dolan, R., 1981. Geomorphology of the Colorado River in Grand Canyon. J. Geol. 89, 269–298.

Jones, H.G., 1992. Plants and Microclimate: A Quantitative Approach to Environmental Plant Physiology, second ed. Cambridge University Press, Cambridge, UK.

Kasten, F., Young, A.T., 1989. Revised optical air mass tables and approximation formula. Appl. Opt. (28), 4735–4738.

Kirk, J.T.O., 1983. Light and Photosynthesis in Aquatic Ecosystems. Cambridge University Press, Cambridge.

Kumar, L., Skidmore, A.K., Knowles, E., 1997. Modeling topographic variation in solar radiation in a GIS environment. Int. J. Geogr. Infor. Syst. 11, 475–497.

List, R.J., 1971. Smithsonian Meteorological Tables. Smithsonian Institution Press, Washington, USA.

McCullough, E.C., Porter, W.P., 1971. Computing clear day solar radiation spectra for the terrestrial environment. Ecology 52, 1008–1015.

Microsoft Corp., 1999. Microsoft Visual Basic for Windows 6.0. Redmond, WA, USA.

Microsoft Corp., 2000. Microsoft Excel for Windows 9.0. Redmond, WA, USA.

Mietz, S.N., Gushue, T., 2002. Colorado River Centerline and Measurement System. USGS, Grand Canyon Monitoring and Research Center, Flagstaff, AZ.

Monteith, J.L., Unsworth, M.H., 1990. Principles of Environmental Physics, second ed. Edward Arnold, London, England.

Mueller, I.I., 1977. Spherical and Practical Astronomy as Applied to Geodesy. Ungar, New York.

Neter, J., Kutner, M.H., Nachtsheim, C.J., Wasserman, W., 1996. Applied Linear Statistical Analysis, fourth ed. Irwin, Chicago, USA.

Page, J.K., Sharples, S., 1988. The SERC Meterological Data Base Volume II: Algorithm Manual, second ed. Department of Building Science, University of Sheffield.

Randle, T.J., Pemberton, E.L., 1987. Results and analysis of STARS (Sediment Transport and River Simulation) modeling efforts of

Colorado River in Grand Canyon. Glen Canyon Environmental Studies Technical Report, NTIS no. PB88-183421.

Rapp, D., 1981. Solar Energy. Prentice-Hall, Inc., Englewood Cliffs, NJ.

Resampling Stats, Inc., 2001. Arlington, Virginia, USA.

Rich, P.M., Hetrick, W.A., Savings, S.C., 1995. Modeling Topographical Influences on Solar Radiation: Manual for the SOLARFLUX model. LA-12989-M, Los Alamos National Laboratories, Los Alamos, NM.

Rosenberg, N.J., Blad, B.L., Verma, S.B., 1983. Microclimate, The Biological Environment. John Wiley & Sons, New York, USA.

Rubin, D.M., Topping, D.J., 2001. Quantifying the relative importance of flow regulation and grain size regulation of suspended sediment transport α and tracking changes in grain size of bed sediment β. Water Resources Res. 37, 133–146.

Schmidt, J.C., 1990. Recirculating flow and sedimentation in the Colorado River in Grand Canyon, Arizona. J. Geol. 98, 709–724.

Schmidt, J.C., Webb, R.H., Valdez, R.A., Marzolf, G.R., Stevens, L.E., 1998. Science and values in river restoration in the Grand Canyon: there is no restoration or rehabilitation strategy that will improve the status of every riverine resource. Bioscience 48, 735–750.

Shaver, M.L., Shannon, J.P., Wilson, K.P., Benenati, P.L., Blinn, D.W., 1997. Effects of suspended sediment and desiccation on the benthic tailwater community in the Colorado River, USA. Hydrobiologia 357, 63–72.

Shannon, J.P., Blinn, D.W., Stevens, L.E., 1994. Trophic interactions and benthic animal community structure in the Colorado River, AZ, USA. Freshwater Biol. 31, 213–220.

Shannon, J.P., Blinn, D.W., Haden, G.A., Benenati, E.P., Wilson, K.P., 2001. Food web implications of ^{*13}C and ^{*15}N variability over 370 km of the regulated Colorado River, USA. Isotopes Environ. Health Stud. 37, 179–191.

Sokal, R.R., Rohlf, F.J., 1995. Biometry the Principles and Practice of Statistics in Biological Research. W.H. Freeman and Company, New York, USA.

Statsoft, Inc., 1997. Statistica for Windows. Version 5.1, Tulsa, OK, USA.

Stevens, L.E., Schmidt, J.C., Ayers, T.J., Brown, B.T., 1995. Flow regulation, geomorphology and Colorado River marsh development in the Grand Canyon, Arizona. Ecol. Appl. 6, 1025–1039.

Stevens, L.E., Shannon, J.P., Blinn, D.W., 1997a. Colorado River benthic ecology in Grand Canyon, Arizona, USA: dam, tributary and geomorphological influences. Regul. Riv. 13, 129–149.

Stevens, L.E., Buck, K.A., Brown, B.T., Kline, N.C., 1997b. Dam and geomorphological influences on Colorado River waterbird distribution, Grand Canyon, Arizona, USA. Regul. Riv. 13, 151–169.

Stine, W.B., Harrigan, R.W., 1985. Solar Energy Fundamentals and Design with Computer Applications. John Wiley and Sons Inc., New York, NY.

Thekaekara, M.P., 1977. Solar irradiance, total and spectral. In: Sayigh, A.A.M. (Ed.), Solar Energy Engineering. Academic Press, New York, NY.

Vanote, R.L., Minshall, G.W., Cummins, K.W., Sedell, J.R., Cushing, C.E., 1980. The river continuum concept. Can. J. Fish Aquat. Sci. 37, 130–137.

Whitton, B.A., 1970. Biology of *Cladophora* in freshwaters. Water Res. 4, 457–476.

Wilson, K.P., Shannon, J.P., Blinn, D.W., 1999. Effects of suspended sediment on biomass and cell morphology of *Cladophora glomerata* (Chlorophyta) in the Colorado River, Arizona. J. Phycol. 35, 35–41.

Walters, C., Korman, J., Stevens, L.E., Gold, B., 2000. Ecosystem modeling for evaluation of adaptive management policies in the Grand Canyon. Conser. Ecol. 4, 1–65.

Yard, M.D., 2003. Light availability and aquatic primary production: Colorado River, Glen and Grand Canyons, AZ. Ph.D. Dissertation. Northern Arizona University, Flagstaff, AZ.